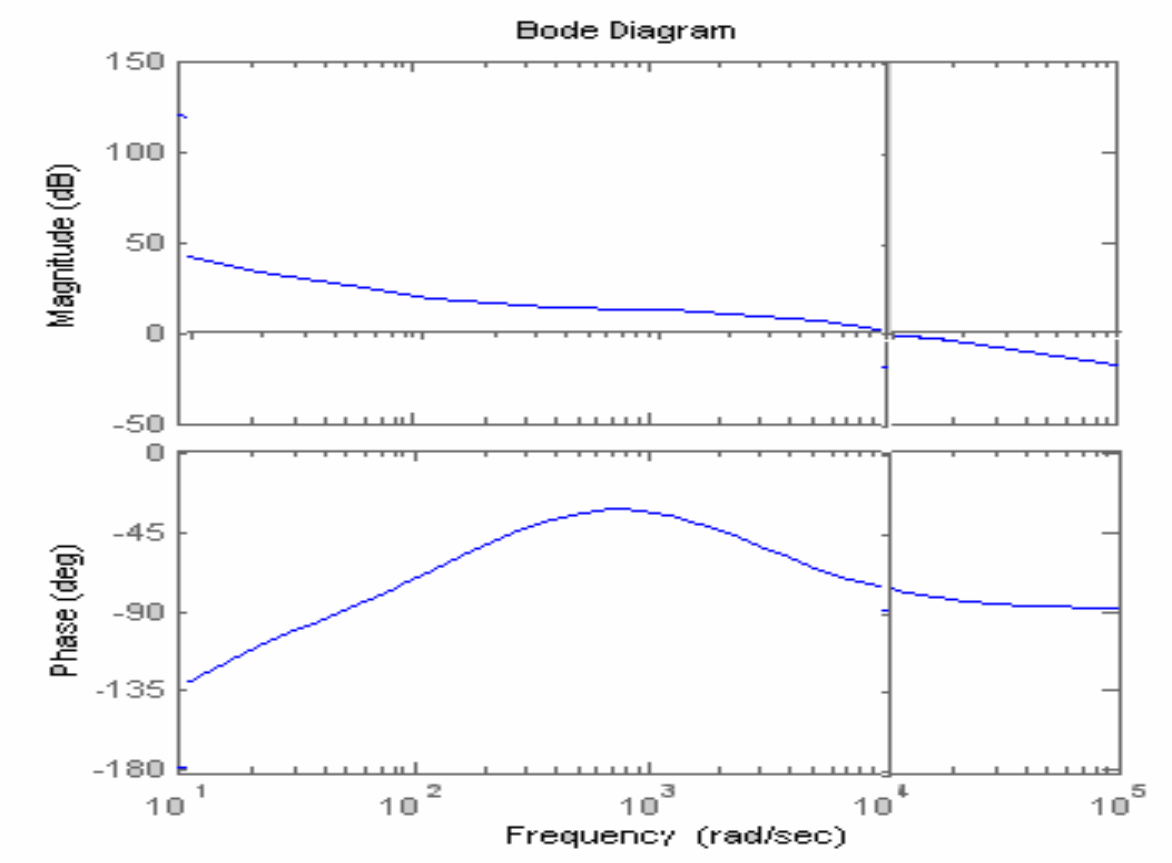

Fig.10 Previous Bode plot of case 1 in Fig. 1.

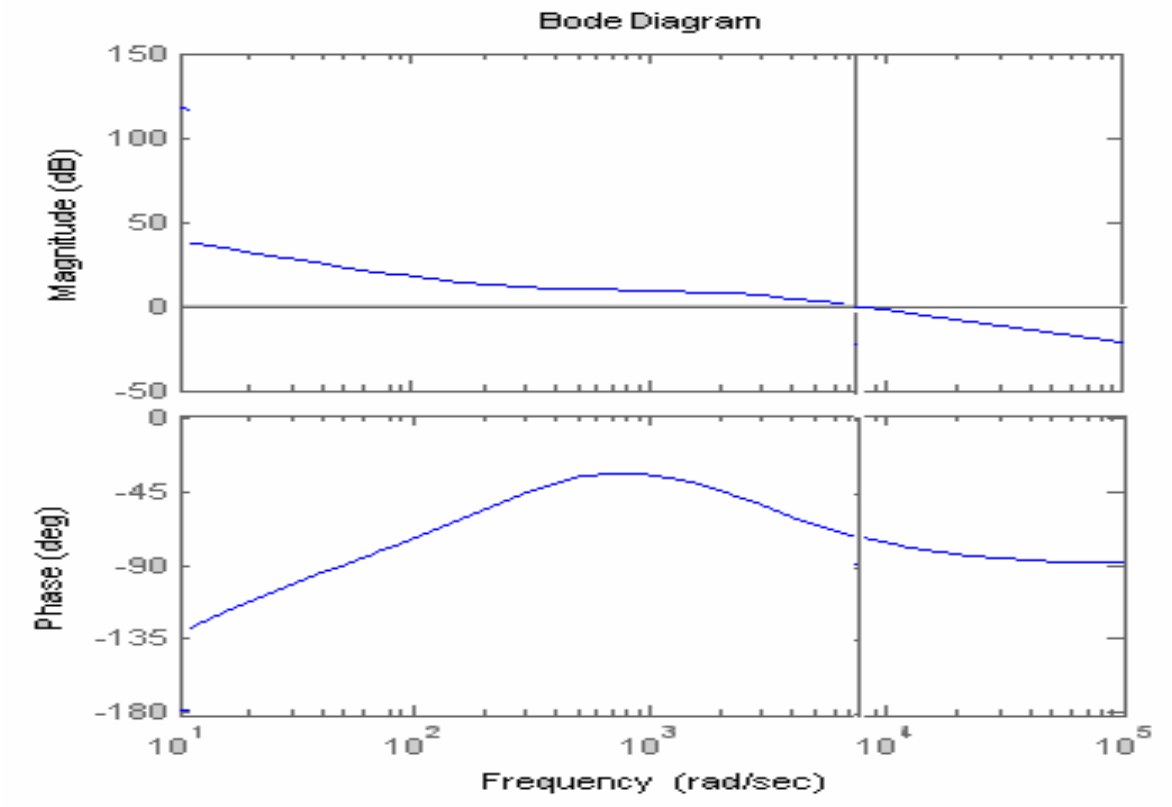

Fig.11 Previous Bode plot of case 2 in Fig. 1.

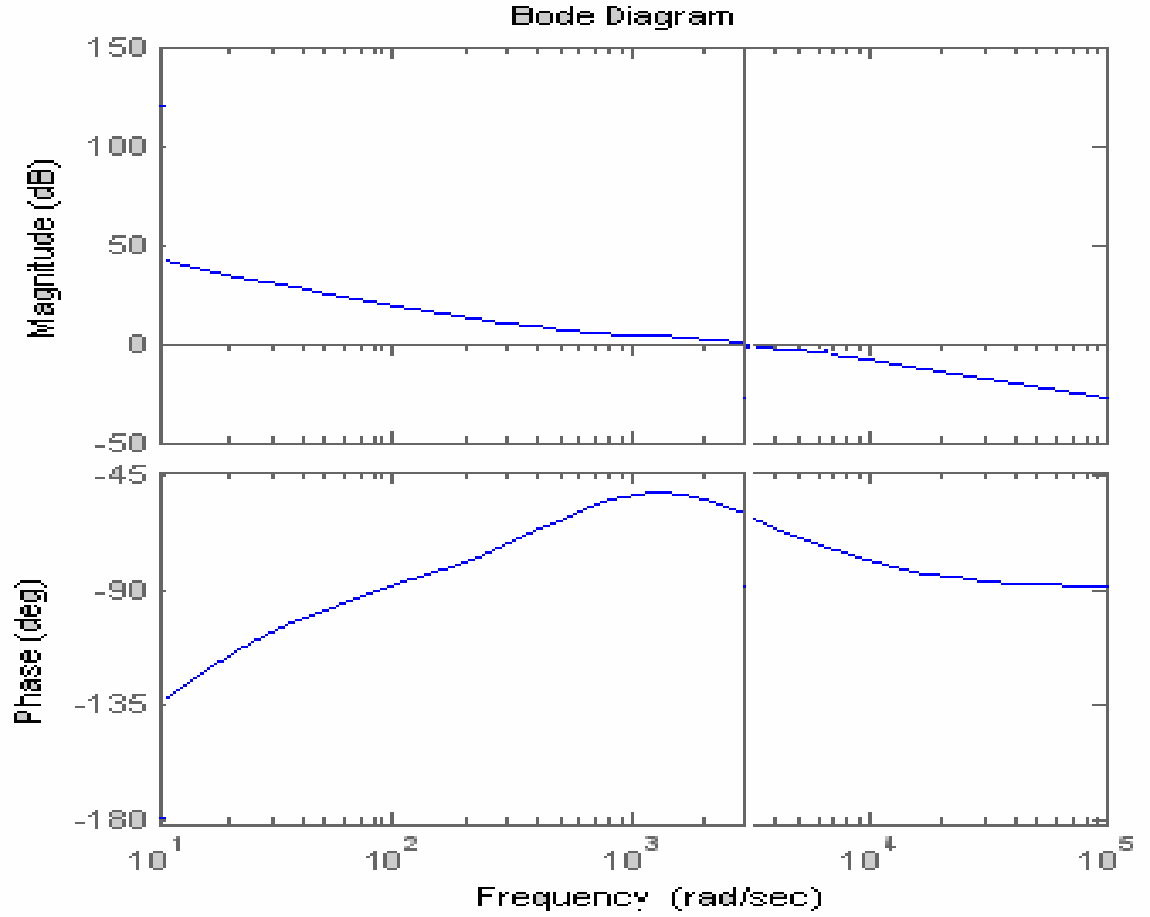

Fig.12 Previous Bode plot of case 5 in Fig. 1.

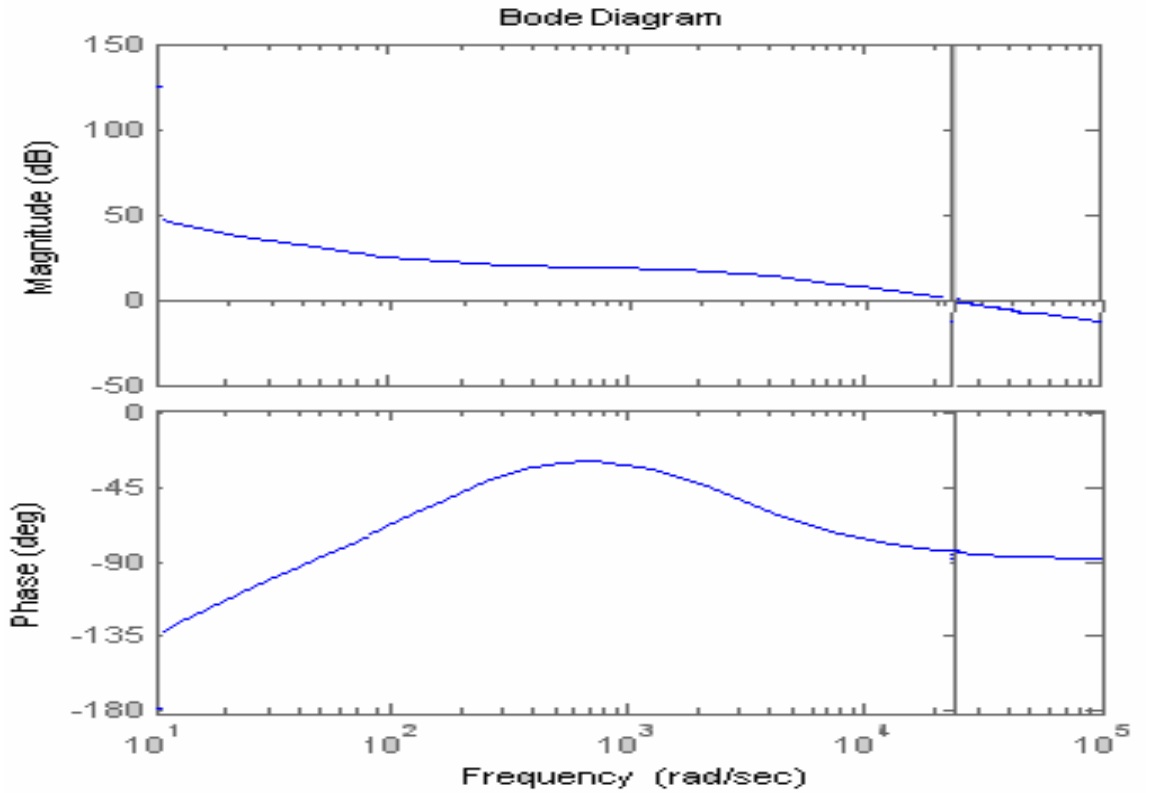

Fig.13 Previous Bode plot of case 6 in Fig. 1.

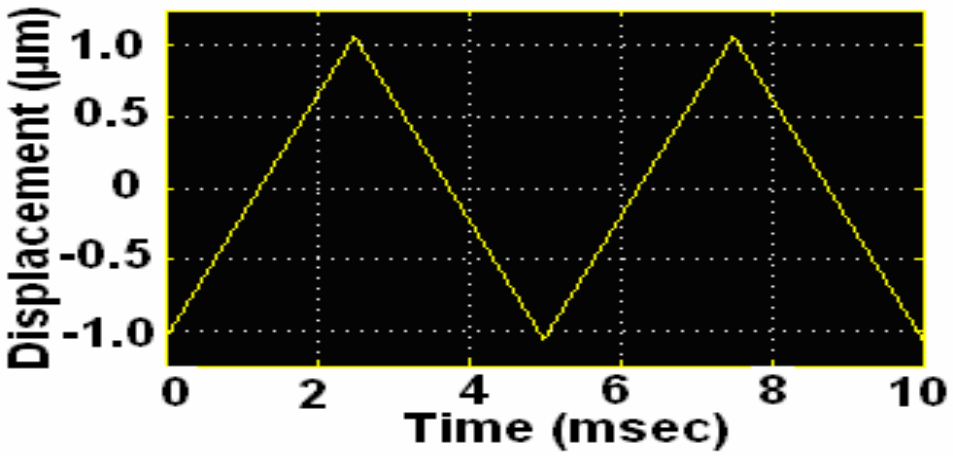

Fig.14 Saw tooth shaped displacement command as input.

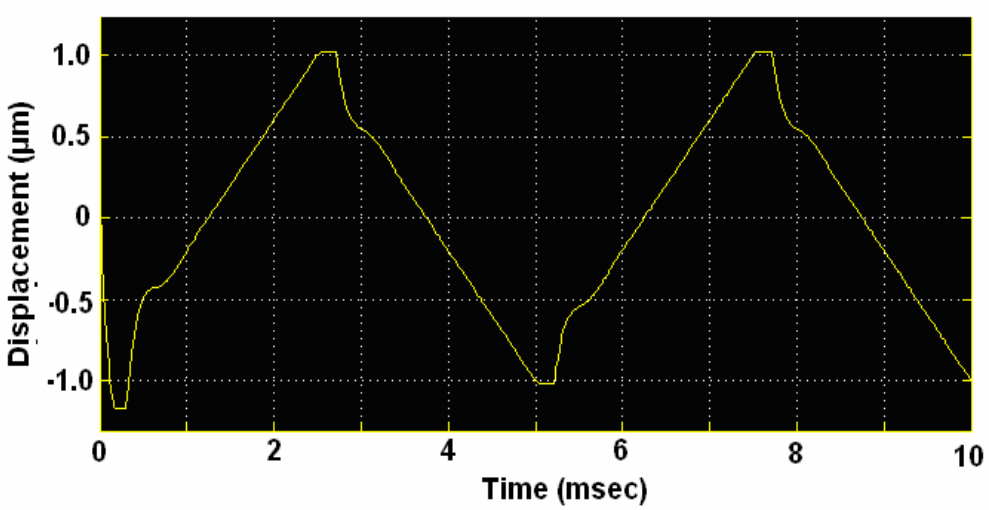

Fig.15 Previous design output of case 1 in Fig. 1.

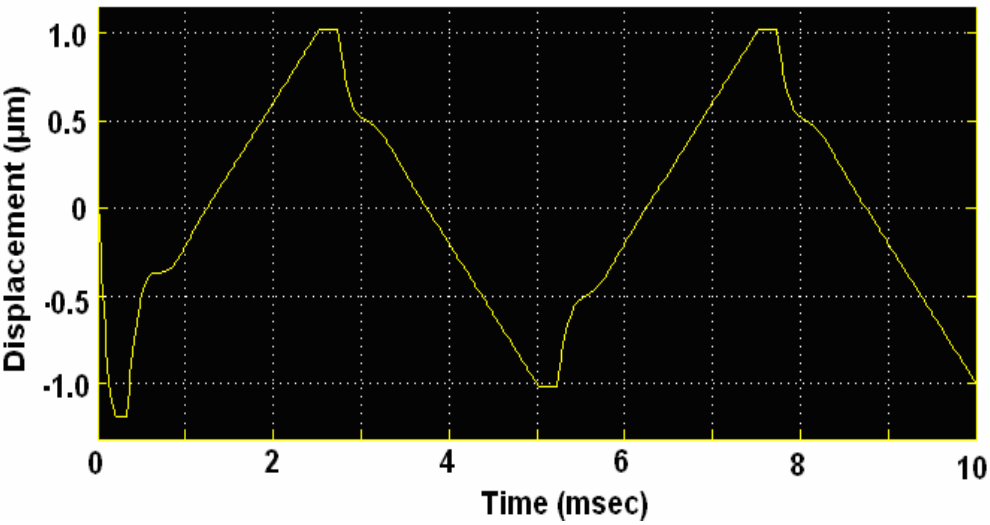

Fig.16 Previous design output of case 2 in Fig. 1.

Now consider the second previous design without LVT for inner-loop feedback in Fig.6. Table 2 also listed the inner and outer loop gains. In addition, the gain margin, phase margin and ω_c are also included. The Bode plots for cases of 1, 3, 4 and 8 are in Figs.19-22 for comparison. In addition, the outputs for saw tooth-shaped input are in Figs. 23-26 (D = 0.3).

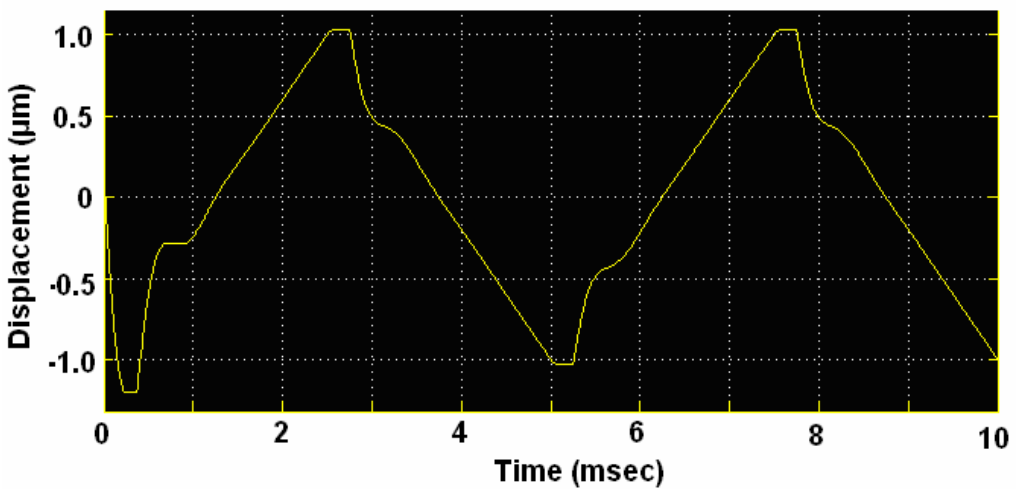

Fig.17 Previous design output of case 5 in Fig.1.

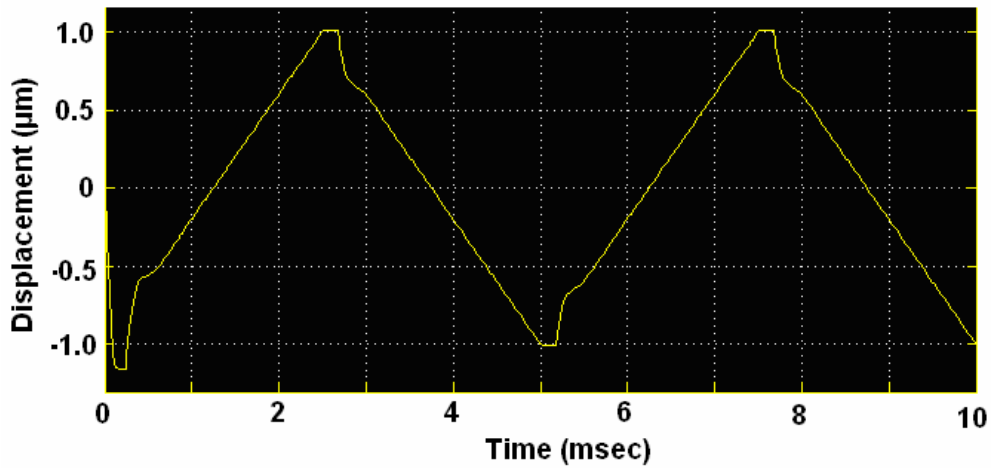

Fig.18 Previous design output of case 6 in Fig.1.

Table 2 The design results of system in Fig.2.

Case	K1	K2	K3	K4	GM	PM (Deg)	ω_c (rad/sec)
1	1	0	1	200	∞	109	80
2	0.5	0	1	200	∞	100	40
3	0.25	0	1	200	∞	98	20
4	0.1	0	1	200	∞	90	8
5	1	0.2	1	200	∞	110	90
6	0.5	0.4	1	200	∞	92	30
7	0.25	0.6	1	200	∞	89	20
8	0.1	0.8	1	200	∞	50	9

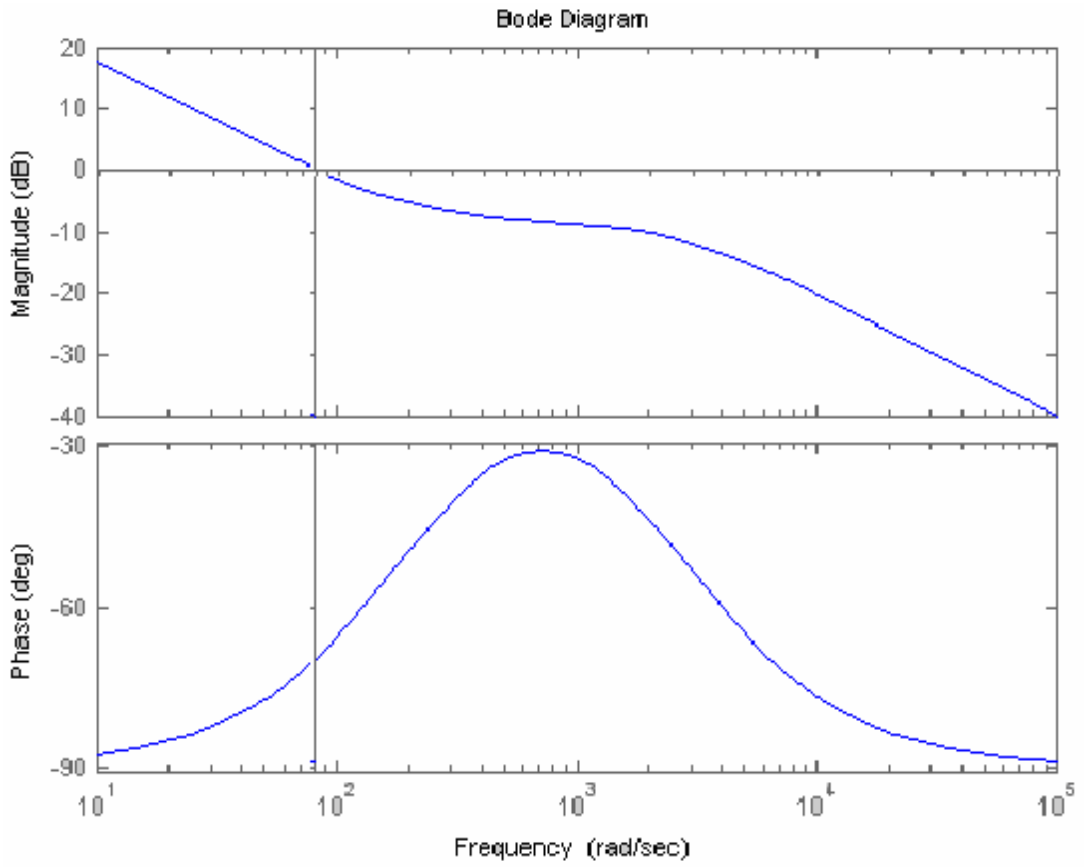

Fig.19 Previous Bode plot of case 1 in Fig.2.

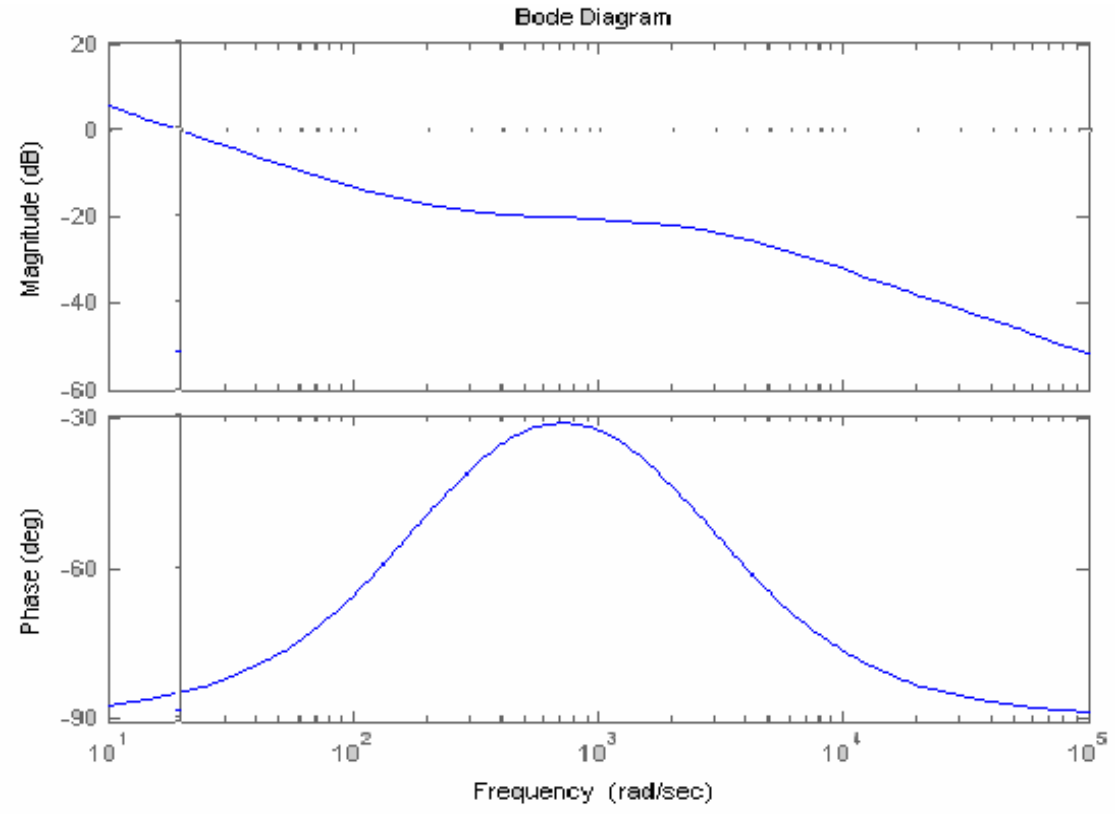

Fig.20 Previous Bode plot of case 3 in Fig.2.

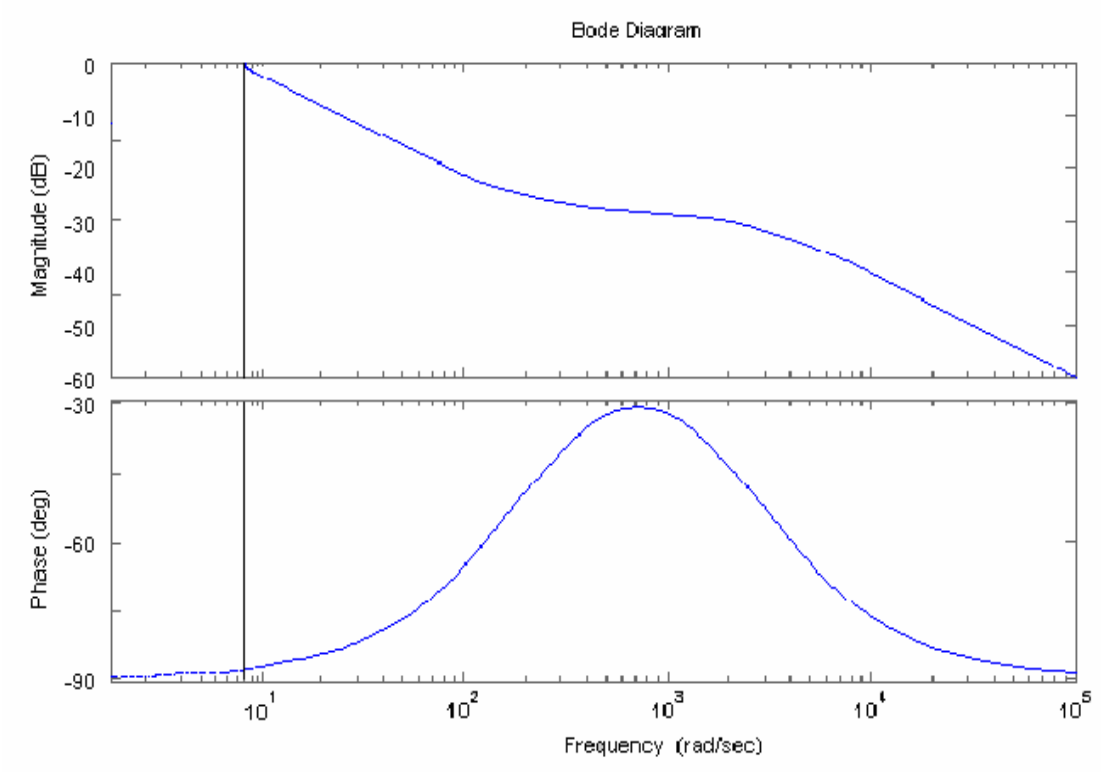

Fig.21 Previous Bode plot of case 4 in Fig.2.

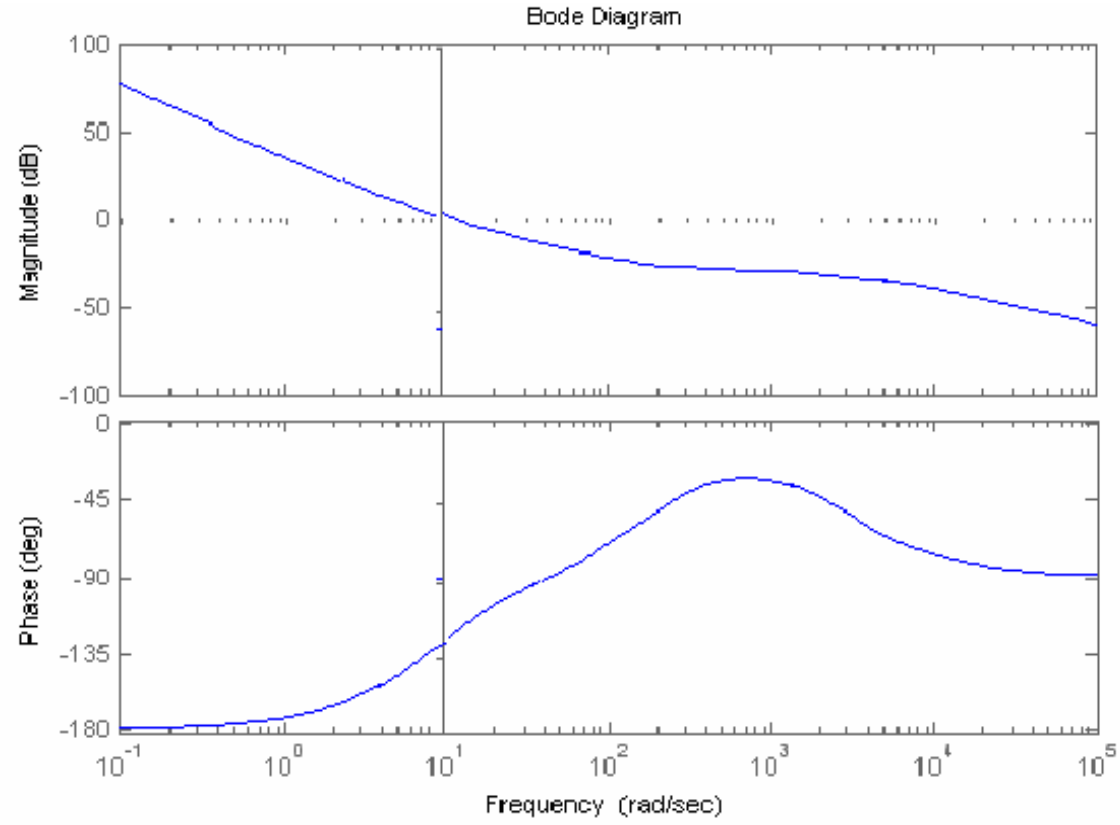

Fig.22 Previous Bode plot of case 8 in Fig.2.

One can see the hysteresis effect is lower for case 1 with larger phase margin, while still bad for cases 3, 4 and 8. The reason is that the phase margins as well as the magnitudes of ω_c are larger for case 1, thus the system responses are quicker, and the dead zone effect and phase delay produced by the hysteresis effect would be smaller as in Fig.23. However, the magnitudes of ω_c as well as the phase margin are much smaller for cases 3 and 4, thus the hysteresis effects are larger as in Figs.24 and 25. In addition, since the original phase margin as well as the magnitudes of ω_c are too smaller of case 8, thus as Fig.26 shows that the stability can even be degraded by adding the hysteresis effect to push the phase margin approaching zero.

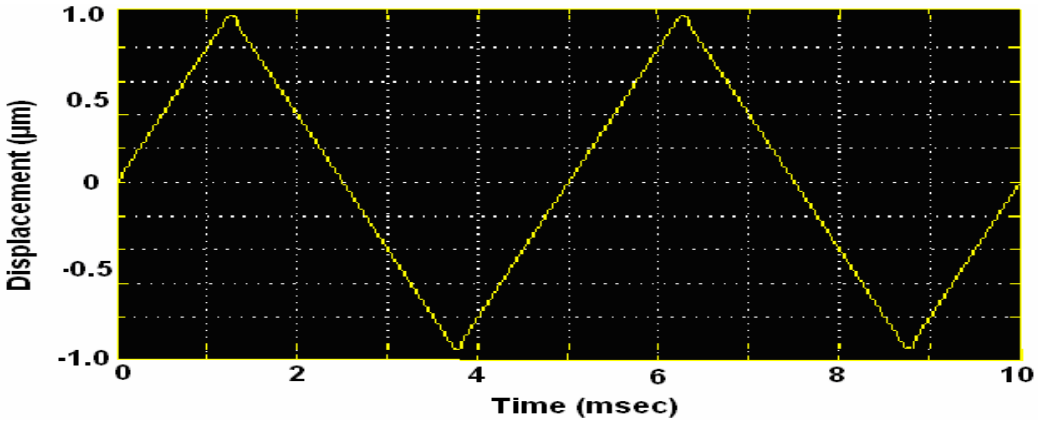

Fig.23 Previous design output of case 1 in Fig.2.

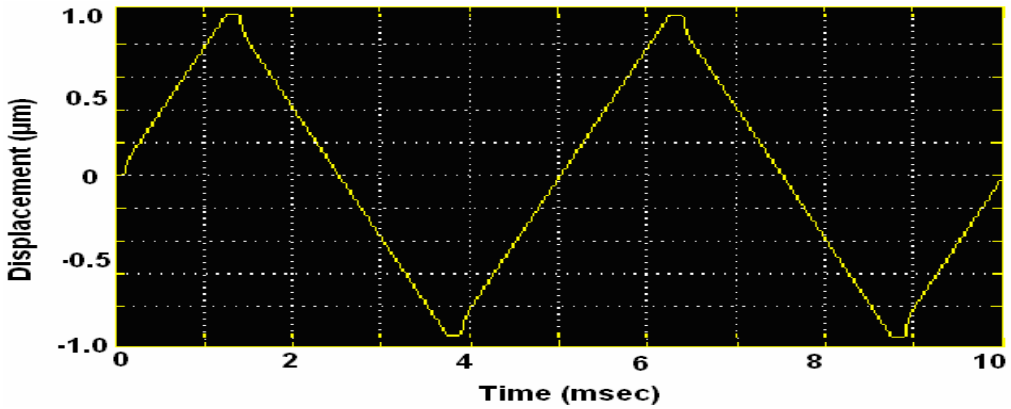

Fig.24 Previous design output of case 3 in Fig.2.

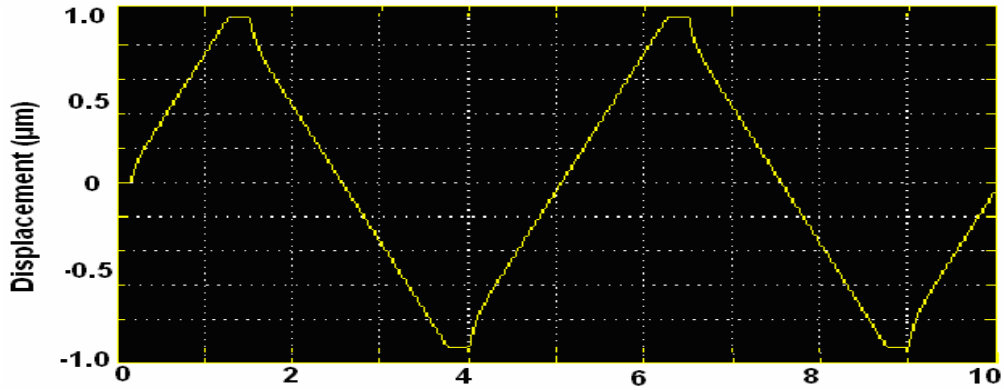

Fig.25 Previous design output of case 4 in Fig.2.

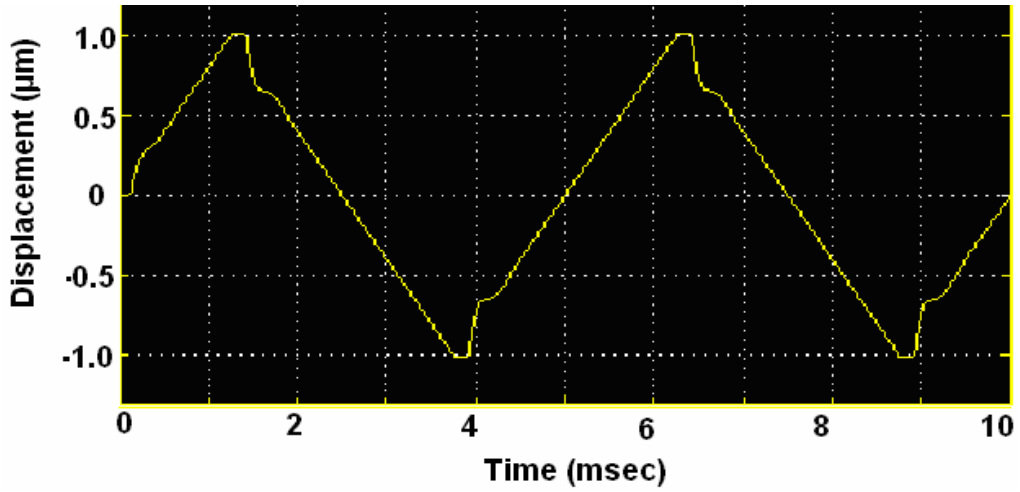

Fig.26 Previous design output of case 8 in Fig.2.

3 Fuzzy Controller Design

3.1 Relationship Functions Design

In this section a Proportion and Derivative (PD) type fuzzy controller [14-18] is applied in the forward loop as in Fig. 3. It is well-known that fuzzy controller is based on the IF-THEN RULE as follows:

R1: IF E is NB AND ΔE is NB THEN U is NB,
R2: IF E is NB AND ΔE is ZE THEN U is NM,
R3: IF E is NB AND ΔE is PB THEN U is ZE,
R4: IF E is ZE AND ΔE is NB THEN U is NM,
R5: IF E is ZE AND ΔE is ZE THEN U is ZE,
R6: IF E is ZE AND ΔE is PB THEN U is PM,
R7: IF E is PB AND ΔE is NB THEN U is ZE,
R8: IF E is PB AND ΔE is ZE THEN U is PM,
R9: IF E is PB AND ΔE is PB THEN U is PB,

where NB, NM, NS, ZE, PS, PM, and PB respectively stand for negative big, negative middle, negative small, zero, positive small, positive middle, and positive big. The detailed cross reference rules for the inputs and the outputs of fuzzy controller are defined in Table 3. According to fuzzy control design method the relationship functions of error E, ΔE (deviations of present E and the previous E), and U (control input) are defined at first, which are listed in Table 4 and shown in Figs.27-29. To reduce the computation time the triangular distribution functions are applied in fuzzy controller relationship functions calculation instead of using the traditional Gaussian ones.

Table 3 Fuzzy controller cross reference rules.

E /Δ*E*	NB	NM	NS	ZE	PS	PM	PB
NB	NB	NB	NM	NM	NS	NS	ZE
NM	NB	NM	NM	NS	NS	ZE	PS
NS	NM	NM	NS	NS	ZE	PS	PS
ZE	NM	NS	NS	ZE	PS	PS	PM
PS	NS	NS	ZE	PS	PS	PM	PM
PM	NS	ZE	PS	PS	PM	PM	PB
PB	ZE	PS	PS	PM	PM	PB	PB

Table 4 Relationship functions of E, ΔE and U.

Item	Parameter E	Parameter ΔE	Parameter U
Negative Big (NB)	[-1 -1 -0.75 -0.3]	[-4.5 -4.5 -3.375 -1.35]	[-12 -12 -9.6 -8.4]
Negative Medium (NM)	[-0.75 -0.3 -0.15]	[-3.375 -1.35 -0.72]	[-9.6 -8.4 -7.2]
Negative Small (NS)	[-0.15 -0.1 0]	[-1 -0.5 0]	[-8.4 -4.8 0]
Zero (ZE)	[-0.05 0 0.05]	[-0.25 0 0.25]	[-4.8 0 4.8]
Positive Small (PS)	[0 0.1 0.15]	[0 0.5 1]	[0 4.8 8.4]
Positive Medium (PM)	[0.15 0.3 0.75]	[0.72 1.35 3.375]	[7.2 8.4 9.6]
Positive Big (PB)	[0.3 0.75 1 1]	[1.35 3.375 4.5 4.5]	[8.4 9.6 12 12]

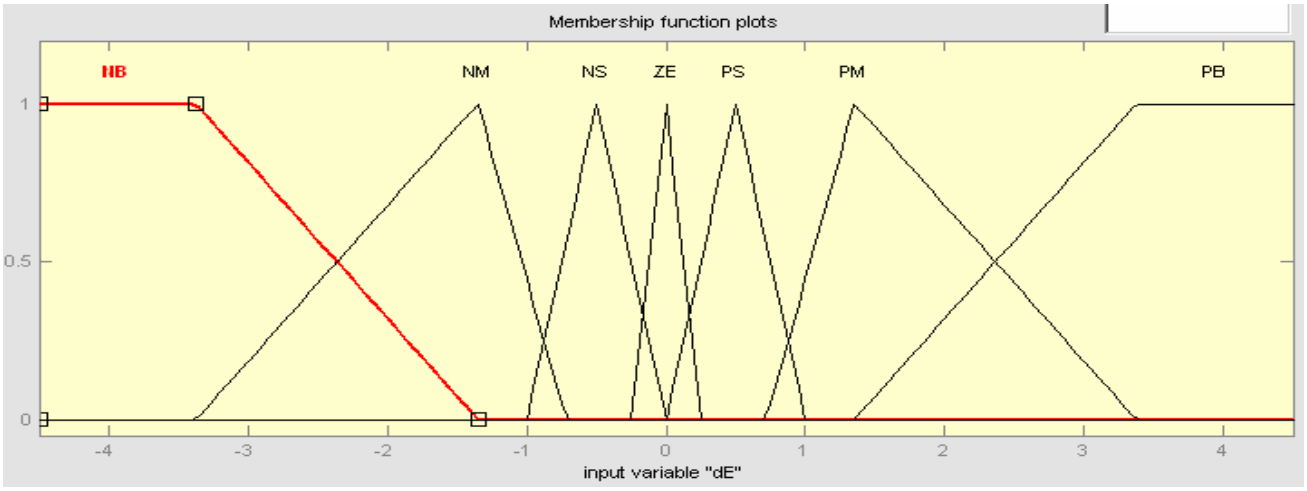

Fig.27 Relationship functions of error E.

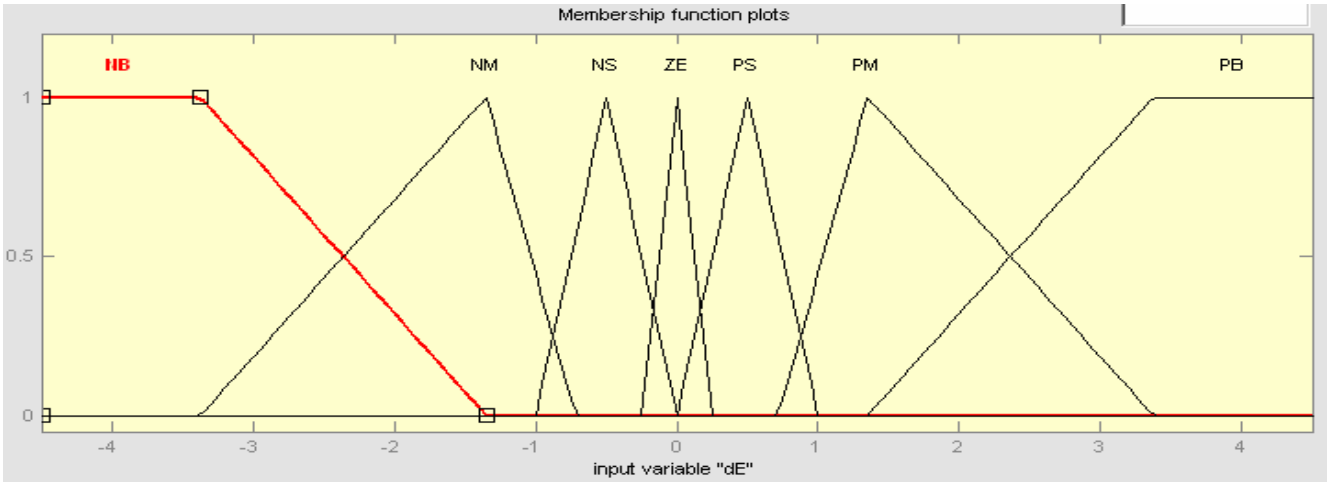

Fig.28 Relationship functions of error rate ΔE.

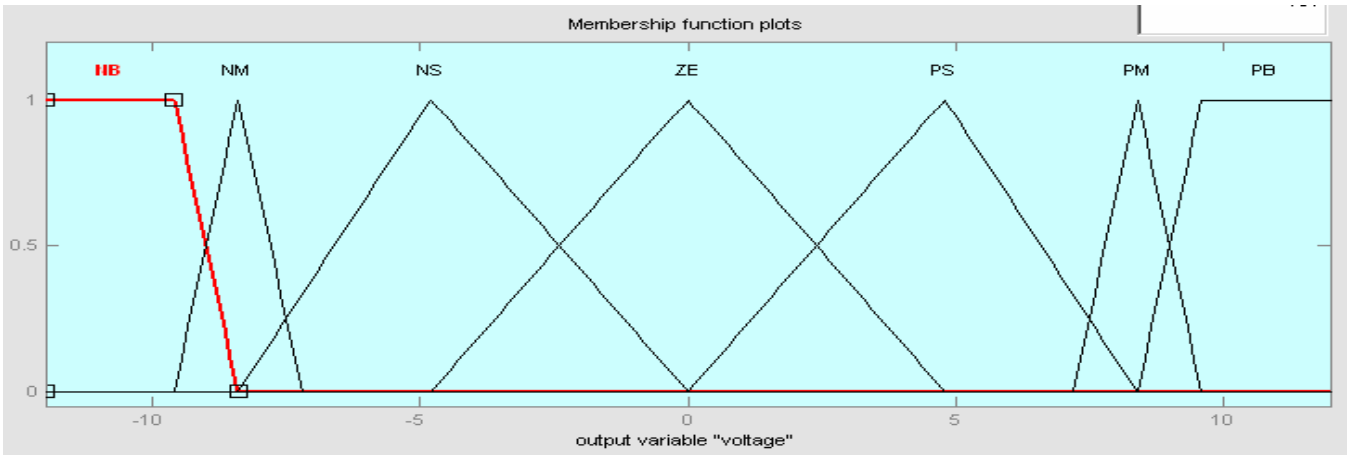

Fig.29 Relationship functions of fuzzy controller output.

3.2 Fuzzy Controller Performance Analysis

Fig 30 shows the response (D = 0.3). It can be seen that the hysteresis effect is almost disappeared, so that this method is better than those obtained by the previous PI controllers. However, there are some chattering effects and can be accomplished by sliding mode control methods [16-18], the result is as in Fig.31.

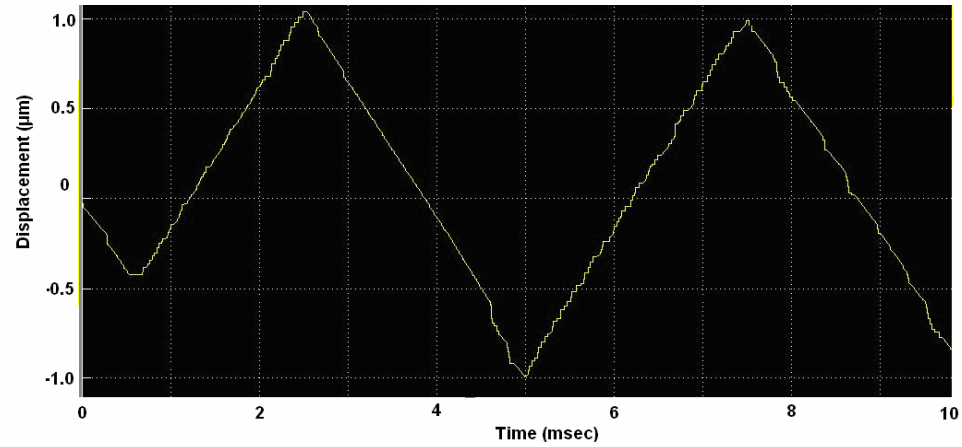

Fig.30 The output response with fuzzy controller.

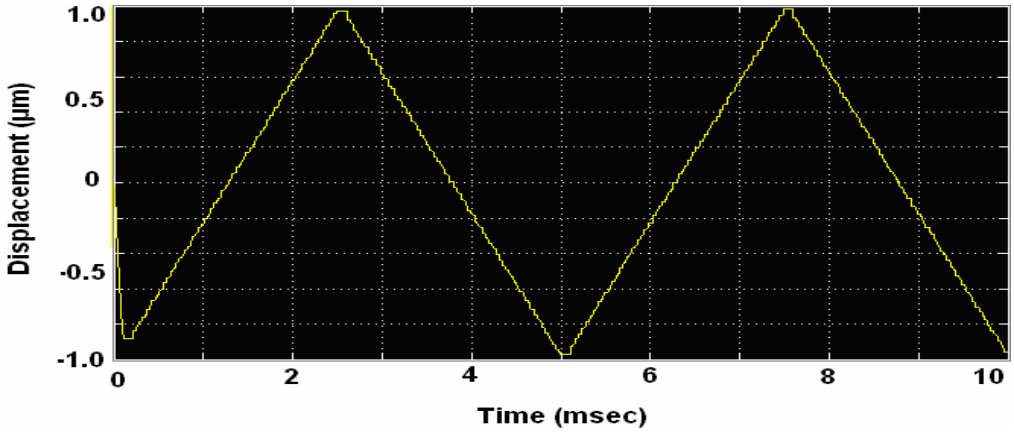

Fig.31 The output response obtained by using fuzzy controller and sliding mode control method.

4 Test Results and Discussions

The signal flow graph of the operation steps is shown in Fig. 32 and summarized as follows. The operation steps are summarized as follows. The first step of test is initial levelling of the balance lever arm, which is achieved by adjusting the current through the coil of force actuator. Since the lever arm weight at the stylus probe (contact with the sample) side is heavier than the other side (contact with actuator) intentionally, thus the force actuator should push down to make the balance lever arm even. The contact point of the lever arm on the load cell is installed right at the calibrated-levelling height. This adjustment process stops when the value of load cell output increases from 0 mg to 100 mg. This value for the weight discrimination can be lowered if the circuit routing condition is better, thus the noise amplitude at the load cell output can be reduced.

The next step is to load the sample on the holder which is fixed on the piezo-stage as well as XYZ-stages, and then setting the XY-stages (the resolution is 34 nm in either axis) to make the first sampled point just right under the tip of the stylus probe, then raising the piezo-stage upward until the sampled point touching with the probe. The value of the probe contact force on the sample can be obtained by the load cell. In order to make sure that the probe contacts with the sample while not destroy it; the maximum contact force is limited to 100 mg. This adjustment process stops when the value of load cell output increases from 0 mg to 100 mg as shown in Fig.33, i.e., if the magnitude of contact force is smaller than 100 mg, then moving the piezo-stage upward by one step (the resolution is 10 nm), otherwise, stop. Then by scanning the XY-stages in either x- or y-axis, and finally, the surface profile of the sample can be obtained as shown in Figs.34 (a) and (b) for side view and top view, respectively. For comparison purpose a commercial profiler (ET-4000) was also applied, the surface profile of which was shown in Fig.35. Thus one can see that the performance of the proposed system was very good.

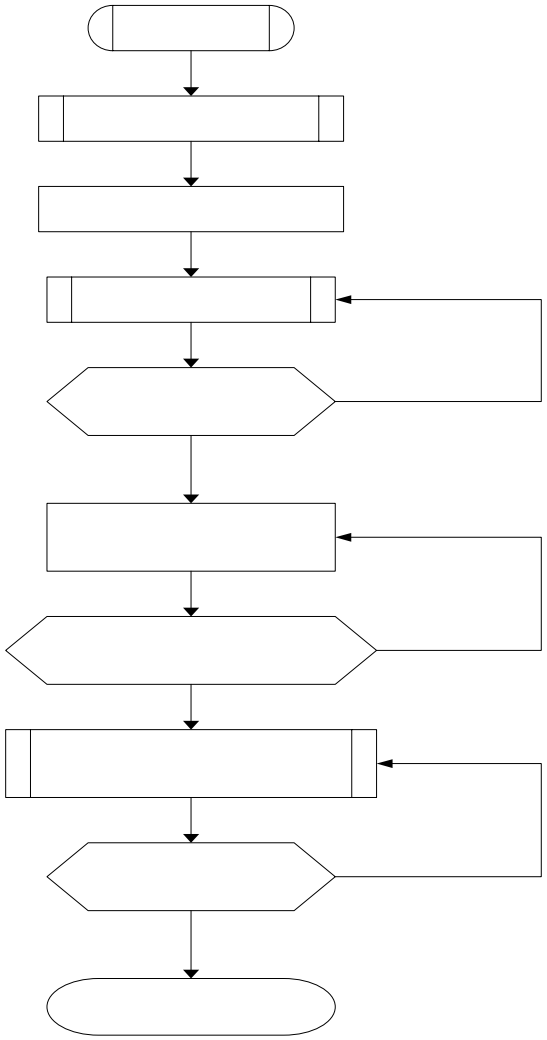

Fig.32 The signal flow graph of the operation steps.

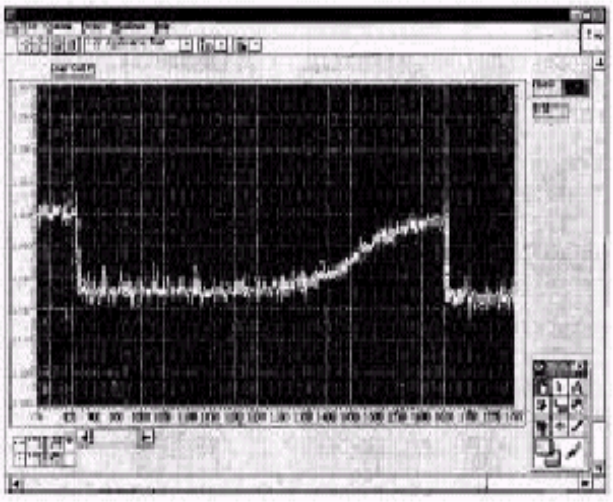

Fig.33 Output voltage of load cell is increased for contact force changing from 0 mg to 100 mg.

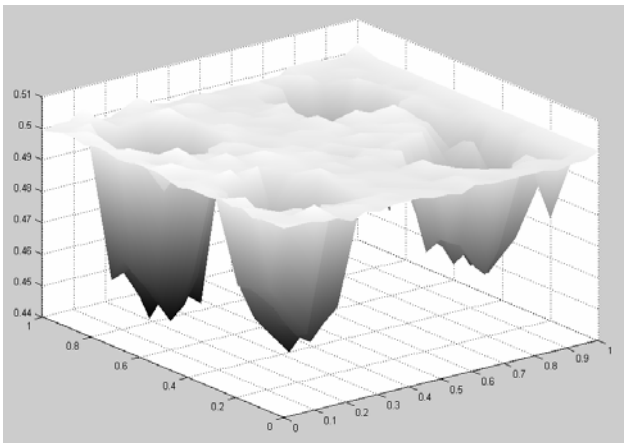

(a) Side view

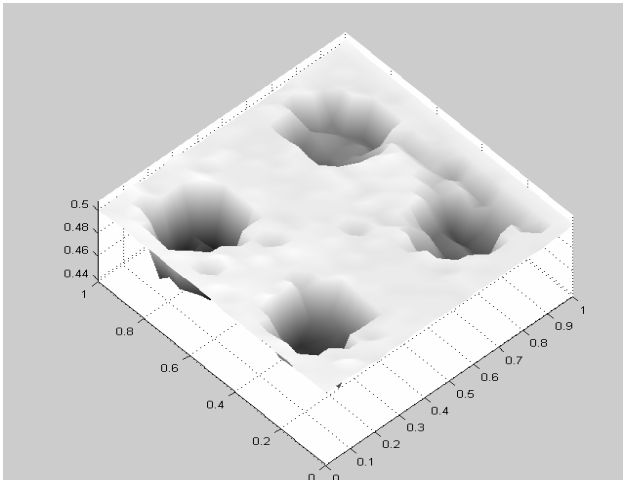

(b) Top view

Fig.34 The surface profile of a sample obtained by the proposed method.

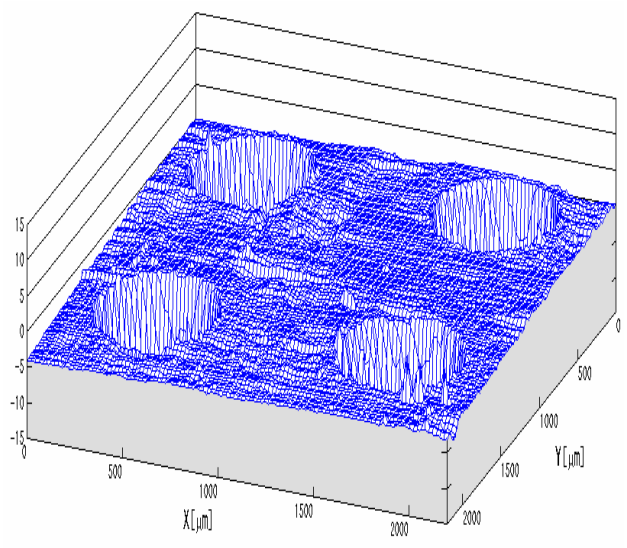

Fig.35 Surface profile of a BGA substrate with a commercial profiler (ET-4000).

5 Conclusion

This research applied fuzzy control method for a Scanning Probe Microscope (SPM) system design. In addition, the actuator hysteresis effect was taken into consideration. Comparisons with two previous works with and without Linear Velocity Transducer (LVT) for inner-loop feedback compensation are also made, it can be seen that the system performance obtained by the fuzzy controller is much better, especially in eliminating the actuator hysteresis effect. This improvement has been verified by MATLAB simulation and practical implementation of a surface profiler. Finally, the profile of the object surface is displayed on a 3D graph.

References:

[1] D. G. Chetwyud, X. Liu and S. T. Smith, A Controlled-force Stylus Displacement Probe, *Precision Engineering*, Vol. 19, No.2/3 October/ November, 1996, pp. 105-111.

[2] X. Liu, D. G. Chetwyud, S. T. Smith, and W. Wang, Improvement of the Fidelity of Surface Measurement by Active Damping Control, *Measurement Science Technology*, 1993, pp. 1330-1340.

[3] G. Neubauer, S. R. Cohen, G. M. McClelland, D. Horne, and C. M. Mate, Force Microscopy with a Bidirectional Capacitor Sensor, *Rev. Science Instrument*, Vol. 61, No.9, 1990, pp. 2296-2308.

[4] M. Bennett, and J. H. Dancy, Stylus Profiling Instrument for Measuring Statistical Properties of Smooth Optical Surfaces, *Applied Optics*, Vol. 20, No.10, 1981, pp. 1785-1802.

[5] D. G. Chetwyud, X. Liu and S. T. Smith, Signal Fidelity and Tracking Force in Stylus Profilometry, *J. of Machinery Tools and Manufacture*, Vol. 32, No.1/2, 1992, pp. 239-245.

[6] M. Bennett, and J. H. Dancy, Stylus Profiling Instrument for Measuring Statistical Properties of Smooth Optical Surfaces, *Applied Optics*, Vol. 20, 1981, pp. 1785-1802.

[7] J. I. Seeger, and S. B. Crary, Stabilization of Statistically Actuated Mechanical Devices, *Electro-Transducers '97*, Chicago, IL, 1981, p. 1133.

[8] G. Haugstad, and R. R. Jones, Mechanisms of Dynamic Force Microscopy on Polyvinyl Alcohol: Region-specific Non-contact and Intermittent Contact Regimes, *Ultra-microscopy*, Vol.76, 1999, pp.77-86.

[9] V. V. Prokhorov, and S. A. Saunin, Probe-surface Interaction Mapping in Amplitude Modulation Atomic Force Microscopy by Iintegrating Amplitude-distance and Amplitude-frequency Curves, *Appl. Phys. Lett.*, Vol. 91, 2007, pp. 1063-1065.

[10] J. M. Lin and C. C. Lin, Profiler Design with Multi-sensor Data Fusion Methods, *SICE Annual Conference 2007 in Takamatsu*, September 17-20, 2007, pp. 710-715.

[11] P. K. Chang and J. M. Lin, Scanning Probe Microscope System Design with Linear Velocity Transducer for Feedback Compensation, *SICE Annual Conference 2008 in Tokyo*, August 20-22, 2008, pp. 2382-2387.

[12] P. K. Chang and J. M. Lin, Scanning Probe Microscope System Design with Fuzzy Control, *Proceedings of the 9th WSEAS International Conference on Automation and Information (ICAI'08), Bucharest, Romania, June 24-26, 2008,* pp. 548-553.

[13] H. C. Tseng and D. W. Teo, Ship Mounted Satellite Tracking Antenna with Fuzzy Logic Control, *IEEE Trans. on Aerospace and Electronic Systems,* Vol. 34, No. 2, 1998, pp. 639-645.

[14] Y. Zhang, G. E. Hearn, and P. A. Sen, A Neural Network Approach to Ship Track-Keeping Control, *IEEE J. of Oceanic Eng ineering,* Vol. 21, No. 4, 1996, pp. 513-527.

[15] H. Zhang and D. Liu, *Fuzzy Modeling & Fuzzy Control,*. New York: Springer-Verlag, 2006.

[16] P. K. Chang and J. M. Lin, Integrating Traditional and Fuzzy Controllers for Mobile Satellite Antenna Tracking System Design, *Proceedings of WSEAS Conference on Advances in Applied Mathematics, Systems, Communications and Computers, selected papers from Circuits, Systems and Signals 2008, Marathon Beach, Attica, Greece,* June 1-3, 2008, pp. 102-108.

[17] G Bartolini, A Ferrara, E Usai, Chattering Avoidance by Second-order Sliding Mode Control, *IEEE Transactions on Automatic Control,* Vol. 43, No. 2, February 1998, pp. 241-246.

[18] W Perruquetti, JP Barbot, *Sliding Mode Control in Engineering*, CRC Press, 2002.